



## Pressure-induced electronic transitions in samarium monochalcogenides

Debalina Banerjee <sup>1,2,\*</sup>, Evgeny Plekhanov,<sup>1</sup> Ivan Rungger <sup>2</sup>, and Cedric Weber<sup>1,3</sup>

<sup>1</sup>*King's College London, The Strand, London, WC2R 2LS, United Kingdom*

<sup>2</sup>*National Physical Laboratory, Teddington, TW11 0LW, United Kingdom*

<sup>3</sup>*Quantum Brilliance, Australian National University, Daley Road, Acton, ACT, Australia*



(Received 9 August 2021; revised 4 March 2022; accepted 6 May 2022; published 23 May 2022)

The pressure-induced isostructural insulator-to-metal transition for SmS is characterized by the presence of an intermediate valence state at higher pressure which cannot be captured by density functional theory. As a direct outcome of including the charge and spin fluctuations incorporated in dynamical mean-field theory, we see the emergence of insulating and metallic phases with increasing pressure as a function of changing valence. This is accompanied by significantly improved predictions of the equilibrium lattice constants and bulk moduli for all Sm monochalcogenides verifying experiments. Nudged elastic band analysis reveals the insulating states to have a finite quasiparticle weight, decreasing as the gap closes rendering the transition to be not Mott-like, and classifies these materials as correlated band insulators. The difference between the discontinuous and continuous natures of these transitions can be attributed to the closeness of the sharply resonant Sm-4*f* peaks to the Fermi level in the predicted metallic states in SmS compared with SmSe and SmTe.

DOI: [10.1103/PhysRevB.105.195135](https://doi.org/10.1103/PhysRevB.105.195135)

### I. INTRODUCTION

An existing present-day challenge is to invent a feasible successor to the complementary metal-oxide semiconductor (CMOS) technology oriented towards increasing computer clock speeds and power performance, whose trends, as per Moore's law [1], have saturated since 2003. This requires arresting of the switching power, which makes us steer towards a different form of technology with nanoscalability where a reduction of line voltage with dimensional scaling increases processor clock speeds. A possible new low-voltage switching and memory element is the piezoelectric transistor (PET) [2]. A PET is essentially a transduction device converting the external voltage to stress in a piezoelectric (PE) material which expands [3] and in turn compresses a piezoresistive (PR) thin film of the order of a few nanometers [4] thereby activating a facile insulator-metal transition. Depending on the nature of the transition, continuous or hysteretic, the device can be used as a switch or a memory element, respectively. It is potentially scalable to nanometers and enables device operations at voltages an order of magnitude lower than CMOS while reducing power by two orders and achieving frequencies up to 10 GHz.

PE materials are well understood and engineered, but the PR materials are more enigmatic. Our work focuses on understanding the electronic origins behind this piezoresistive transition at equilibrium in two primary candidates, viz., SmS [5] for PR sensors and memory applications and SmSe [6] for switching operations. We also study SmTe belonging to the same family and look for trends across these materials originating in electronic structure. Experimental observations have indicated that with pressure the band gap between Sm-4*f*

and Sm-5*d* bands decreases and an isostructural electronic transition occurs from the Sm<sup>2+</sup> state to the Sm<sup>3+</sup> state with an associated mixed valent state occurring discontinuously for SmS [7] and continuously for SmSe and SmTe which indicates the outset of metallic behavior [8]. Along with it, SmSe and SmTe show a reversible change in resistivity, but SmS shows hysteresis [9,10].

Samarium (Sm:[Xe]4<sup>6</sup>s<sup>2</sup>) is a lanthanide with open 4*f* shells. The physical properties of such materials result from an interplay between structure, dimensionality, and strong electronic correlations. Sm monochalcogenides have been studied with first-principles approximations to varying degrees over the course of years. While the density functional theory (DFT) [11,12] with local spin-density approximation (LSDA) [13] falsely predicts the systems to be metallic while largely underestimating the lattice constants, the LSDA+*U* approach with a tunable *U* correctly predicts the band gaps under ambient conditions but fails to capture the mixed valent high-pressure golden phase of SmS between 6 and 20 kbar. A self-interaction corrected (SIC) LSDA [14] shows better predictions for the high-pressure intermediate valence state, but it needs to correct for the theory-predicted energetics in the trivalent configuration and describes the system with a total Sm-4*f* occupation between 5 and 6 by considering it as an array of Sm-*f*<sup>5</sup> ions with one extra partially occupied *f* band [15,16]. Another DFT approach gives better predictions of the lattice constants and bulk moduli by incorrectly making the Sm ions ferromagnetic [17].

The high-pressure cohesive properties have also been studied using three-body interaction potential models [18,19] including long-range Coulomb forces, short-range overlap repulsive forces, and the polarizability effect [20] explicitly up to the next-nearest-neighbor ions, and valence transitions have been studied using model Hamiltonians [21] to various

\*Corresponding author: [debalina.banerjee@kcl.ac.uk](mailto:debalina.banerjee@kcl.ac.uk)

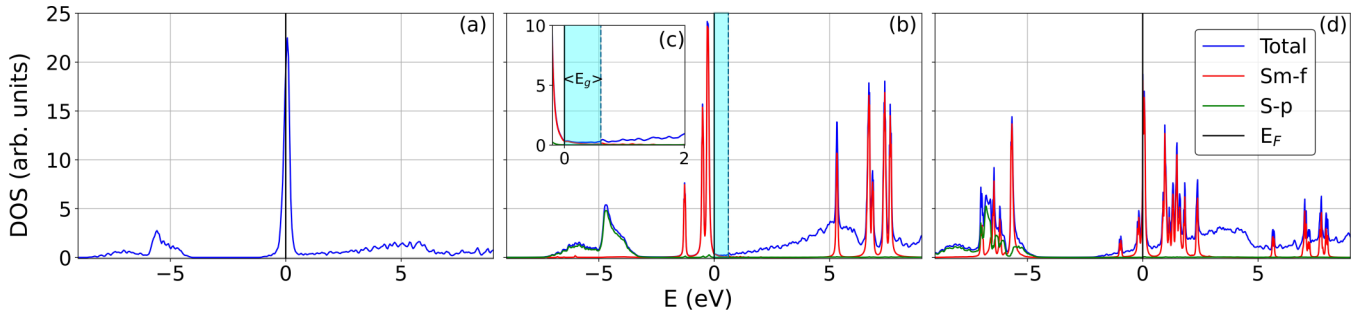


FIG. 1. Density of states (DOS) for SmS obtained with (a) DFT, (b) DFT+DMFT for the Sm-4 $f^6$  configuration corresponding to the ambient pressure insulating black phase [(c) is a magnified version of (b) showing the existence of a finite band gap], and (d) DFT+DMFT for the configuration corresponding to the onset of high-pressure metallicity with intermediate Sm-4 $f$  valence of 5.24(2) in the golden phase.

extents. On the other hand, the standard model of lanthanides [22] puts the  $f$  levels in the core. All this still leads to incorrect predictions of conductance and transmission. Overcoming these obstacles entails the necessity of treating the  $f$  levels with a full many-body Hamiltonian beyond DFT [23], leading to the use of dynamical mean-field theory (DMFT) [24–26] corrections on top of DFT, and using a DFT+DMFT [27] approach to obtain the correct physics. This realistic application of dynamical mean-field methodology has been widely successful for cases where correlation effects are intrinsically accountable for a phenomenon that cannot be explained by the usual band theory arguments. Phase transitions and crossovers between metallic and paramagnetic insulators driven by temperature as in VO<sub>2</sub> [28,29] and V<sub>2</sub>O<sub>3</sub> [30], pressure as for 3d-transition metals and compounds [31], or doping as in Cr-doped V<sub>2</sub>O<sub>3</sub> [32] constitute one class that falls in this category. DMFT has been previously employed with the symmetrized finite- $U$  noncrossing approximation (SUNCA) [33] to study the temperature dependence of SmS and reports a pseudogap appearing near the Fermi level with lowering of temperature after the fashion of Kondo-mixed-valent semimetallic systems.

Trailing the aforementioned motivations, in this paper we aim to provide fully *ab initio* structural predictions, accounting for the many-body effects, within the DFT+DMFT approach. This is key for this class of materials, as they undergo structural and electronic transitions induced under driven pressure. Our approach allows us to disentangle the structural and electronic aspects; in particular, we recover excellent agreement with known experimental parameters, which validates our approach. Lastly, we highlight that the metal-insulator transition is not driven by charge localization (i.e., is not Mott-like), a key result for understanding the physics of this class of systems, and although the Kondo-like physics is important, we find that the gap is dominated by the spectral weight of Sm-5 $d$  electrons, which is dependent on the chalcogenides S, Se, and Te. The emergence of these results will be addressed in detail in the following sections.

This paper is organized as follows: It begins with the Introduction in Sec. I. In Sec. II we discuss the computational details of the investigation, followed by Sec. III, where we analyze how the DFT+DMFT formalism elucidates the above observations. Finally, in Sec. IV we conclude our findings.

## II. COMPUTATIONAL DETAILS

Sm monochalcogenides (Sm $X$ ) form fcc lattices with Sm at (0,0,0) and  $X$  (= S, Se, Te) at (0.5,0.5,0.5). The observed isostructural insulator-to-metal transition in Sm $X$  induced by a change in pressure is concomitant with a change in valence which is experimentally characterized by going from the Sm<sup>2+</sup> state at ambient pressure to the Sm<sup>3+</sup> state at higher pressures. *Ab initio* calculations using DFT, as implemented in the plane-wave basis code CASTEP [34,35], are done with the Perdew-Burke-Ernzerhof functional revised for solids (PBEsol) [36], the Fermi-Dirac smearing scheme with a smearing width of 0.05 eV, and a  $19 \times 19 \times 19$  Monkhorst  $k$  grid [37]. They always converge to a metallic ground state with Sm-4 $f$  peaks at the Fermi level [Fig. 1(a)]. Consistent with the literature, using a tunable  $U_{\text{eff}}$  value shifts the Sm-4 $f$  levels accordingly and leads the system to the correct insulating ground state. It, however, fails to reproduce the metallic state at higher pressures. As there is a change in valence, it is likely that this metal-insulator transition (MIT) is accompanied by intermediate valence states which are not well captured by DFT, it being in principle a single-Slater-determinant approach. The presence of strongly correlated Sm-4 $f$  peaks at the Fermi level are key to these experimentally observed intermediate valence states leading to the onset of metallicity. To capture this fractional occupation state, we look beyond such mean-field approximations warranting the need for many-body corrections.

DMFT has traditionally been a good tool to describe such MITs. Since the 4 $f$  series is usually characterized by a small hybridization, DMFT is used here within the scope of the Hubbard-I (HI) approximation. Thus the Hubbard-I solver [38] as implemented in CASTEP is used with the ensemble density functional method to perform DMFT calculations at various values of lattice constant and valence. We set the inverse temperature  $\beta = 20$  and use 2048 Matsubara frequencies to calculate the Green's functions under the fully localized limit (FLL) approximation for the double-counting correction scheme that adjusts for the Hartree shift already accounted for in DFT. We use a Hund's coupling of  $J = 0.3$  eV (Fig. 5) and a standard value of  $U = 6.1$  eV on Sm at the DMFT level. We find that for the correct ordering of  $X$ - $p$  levels with respect to the Sm-4 $f$  states in the metallic phase, a static DFT- $U$  of 6 eV has to be put on  $X$ . For the insulating state

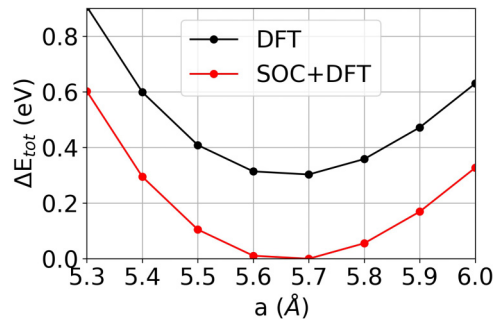


FIG. 2. Total energy  $E_{\text{tot}}$  curves obtained using density functional theory plotted as a function of the lattice constant  $a$  for SmS as implemented in the plane-wave basis code VASP [39,40] using the projector augmented wave (PAW) [41,42] PBE [43] potentials with and without spin-orbit coupling (SOC) [44] optimized with the conjugate gradient algorithm for each value of  $a$  with the energy cutoff of 520 eV, a  $19 \times 19 \times 19$  Monkhorst  $k$  grid [37], and a smearing of 0.05 eV with the tetrahedron method and Blöchl corrections.

this  $U$  does not change the physics qualitatively around the Fermi level other than an expected small shift in the occupied  $p$  states and thus has been used throughout consistently.

Although Sm chalcogenides are heavy fermionic systems, where the spin-orbit coupling (SOC) is expected to play an important role [33] especially in the excitation properties, here we are interested in the structural and integral properties such as total energy, and the SOC contribution to the total energy can be safely neglected, in analogy to how it is done in the standard DFT calculations (Fig. 2). The reason for this is the smallness of the SOC energy scale in comparison with the Coulomb repulsion energy of Sm- $4f$  electrons, and the latter dominates the structural physics of Sm $X$ . Also, note that by solving for a larger subspace, we capture both the  $4f_{5/2}$  and  $4f_{7/2}$  multiplets without identifying them explicitly in our implementation of the DMFT solver [38].

### III. RESULTS

DMFT gives us a control over the degree of correlation and valence of the system across this transition. We capture the effect of pressure via the nominal occupancy  $n_{if}$  which characterizes the Sm- $4f$  electronic valence and is controlled by the double-counting correction as implemented in the HI solver. We then perform energy minimizations to reach the electronic ground state. A clear distinction between insulating [Figs. 1(b) and 1(c)] and metallic [Fig. 1(d)] behaviors emerges for SmS across the MIT as the system goes from ambient to high pressure. This is accompanied by a charge difference of 0.76, which confirms the presence of an intermediate valence state for this material and matches reasonably well with the experimentally observed values of 0.62 [10,45]. The density of states (DOS) for the SmS black phase matches well the observed angle-resolved photoemission spectroscopy (ARPES) spectra [46]. Additionally, with DMFT corrections, the subtle effects due to the paramagnetic nature of SmS also emerge associated with the presence of a local fluctuating magnetic moment between 1.96 and 2.12  $\mu_B$ , not well captured by DFT.

TABLE I. Comparison of experimental data [5,45,49,50] with DFT and DMFT predictions for lattice constant  $a$  and bulk modulus  $B_0$  for SmS, SmSe, and SmTe, along with DMFT-predicted Sm- $4f$  electron occupation  $n_f$ .

Material	$a_{\text{expt}}$ (Å)	$a_{\text{DFT}}$ (Å)	$a_{\text{DMFT}}$ (Å)	$n_f$	$B_{0\text{-expt}}$ (GPa)	$B_{0\text{-DMFT}}$ (GPa)
SmS	5.97 <sup>a</sup>	<sup>b</sup>	5.82 <sup>a</sup>	6.00(2) <sup>a</sup>	89.8–92	90.6
	5.7 <sup>b</sup>	5.54 <sup>b</sup>	5.68 <sup>b</sup>	5.24(2) <sup>b</sup>		
SmSe	6.19 <sup>a</sup>	5.78 <sup>b</sup>	6.14 <sup>a</sup>	6.00(2) <sup>a</sup>	40 ± 5	62.5
SmTe	6.58 <sup>a</sup>	6.20 <sup>b</sup>	6.45 <sup>a</sup>	6.00(2) <sup>a</sup>	40 ± 5	49.5

<sup>a</sup>Insulating state.

<sup>b</sup>Metallic state.

We minimize the DMFT-obtained total energies to relax and optimize the structures which provide the lattice parameters and Birch-Murnaghan [47,48] fitted values of bulk moduli reported in Table I; these values show significant quantitative improvements over DFT predictions and agree well with experiments [5,50] (Fig. 3) for all three Sm $X$  materials. At the onset of the golden phase of SmS we predict a noninteger occupancy of 5.24(2), and of 6.00(2) at the beginning of all the insulating states. Note, however, that in contrast with previous studies, where long-range magnetic order [17], spin-orbit coupling [33], or next-nearest neighbor interactions [19,20] were invoked to reproduce experiments, in this paper we recover consistent results with experimental observations without the need of further mechanisms at room temperature. Although PBEsol underestimates the lattice parameters, we obtain remarkable experimental agreement arising from local charge and spin fluctuation corrections using DMFT.

In the insulating states we find the band gap to increase by approximately 50% and then 20% when going down from isovalent SmS to SmSe to SmTe [Figs. 4(a), 4(c), and 4(e), respectively; see also Fig. 5]. However, even with increasing mass and more electrons, the qualitative nature of the DOS remains essentially the same with some little changes mostly regarding the occupied  $X$ - $p$  levels shifting towards the Fermi level. For the metallic states, we observe the sharp  $4f$  peaks to be almost on top of the Fermi level within 0.01 eV for SmS, and just across it within 0.1 eV for SmSe and SmTe shifting towards the right as we go down the group [Figs. 4(b), 4(d), and 4(f), respectively]. These shifts can be attributed to the previously noted increase in band gap, which pushes the  $f$  states further above the Fermi level and is consistent with experimental observations [50], and might explain the difference between the discontinuous nature of the MIT in SmS and its continuous nature in SmSe and SmTe. This very sharp resonance is crucial to the onset of metallicity as small differences in pressure, temperature, or disorder might shift this peak to left or right and cause huge changes in the density at the Fermi level making its position a critical parameter for transport and calorimetry. A point to note here is that the metallic states for SmSe and SmTe have not been observed in experiments. This can be regarded as a utility of DMFT as we can hereby predict properties of systems which are not fully stabilized in experiments and can use this to gauge the effect of mass contrast in these systems.

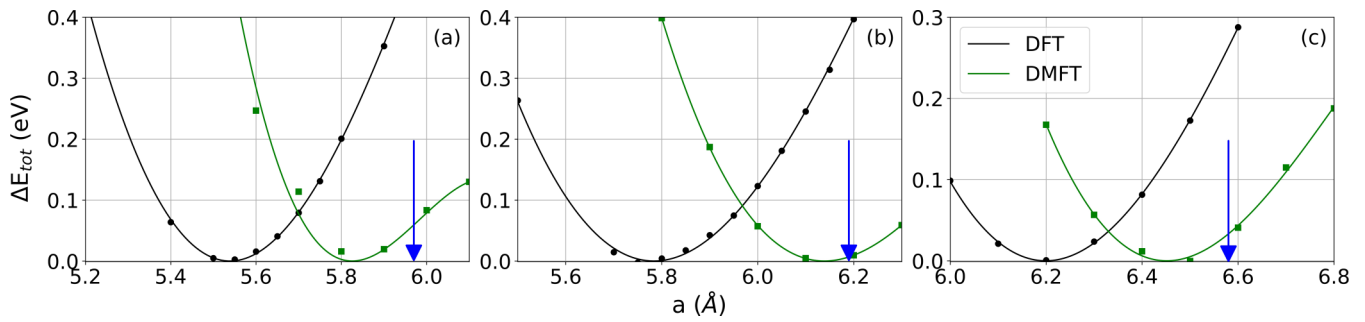


FIG. 3. Comparison between DFT and DFT+DMFT predictions of total energy  $E_{\text{tot}}$  curves plotted as a function of lattice constant  $a$  and fitted with a Birch-Murnaghan [47,48] equation of state for (a) SmS, (b) SmSe, and (c) SmTe. Arrows show the experimentally observed values for the respective lattice constants under ambient conditions.

These systems are composed of weakly hybridized  $4f$  magnetic moments. However, note that the gap in these systems is not Hubbard-like, but is instead between the  $4f$  states and the  $5d$  states. To a large degree, the gap is controlled by the bandwidth of these  $5d$  states. The bandwidth of the upper band is dependent on the chemistry of the chalcogenides and is approximately 7, 6, and 5 eV for SmS, SmSe, and SmTe,

respectively. The  $4f$  states, however, are very much atomiclike and, as seen in our calculations, remain very similar across the three materials.

To investigate the nature of the MIT further, we employ the nudged elastic band (NEB) method [51]. We select a path from the predicted DMFT solution for the insulating ground states corresponding to the larger value of lattice constants

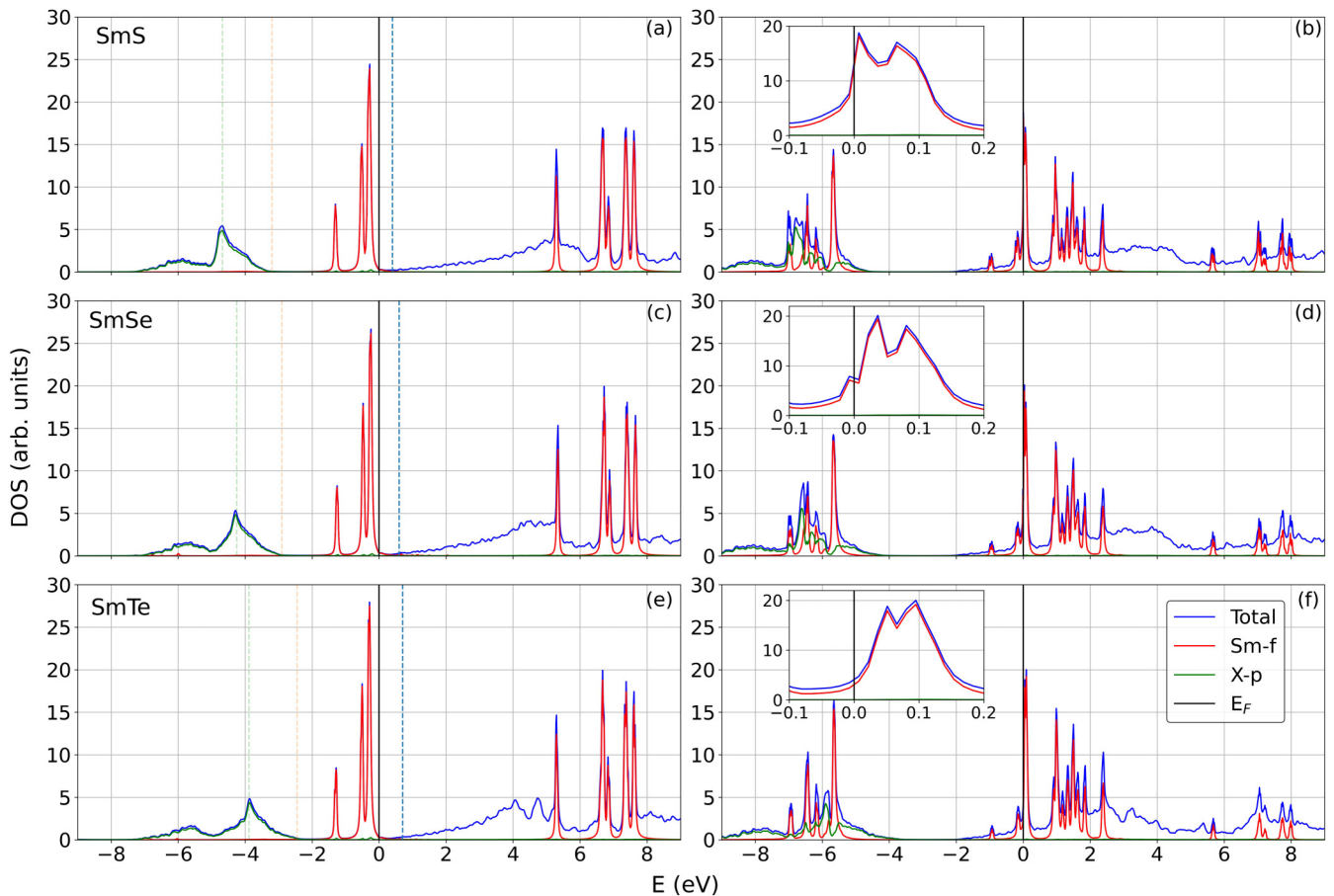


FIG. 4. Left column: density of states obtained with DFT+DMFT corresponding to the ambient pressure insulating states for (a) SmS, (c) SmSe, and (e) SmTe. Right column: the high-pressure intermediate valence metallic states with insets focusing on the behavior of Sm- $4f$  peaks around the Fermi level for (b) SmS, (d) SmSe, and (f) SmTe, respectively.

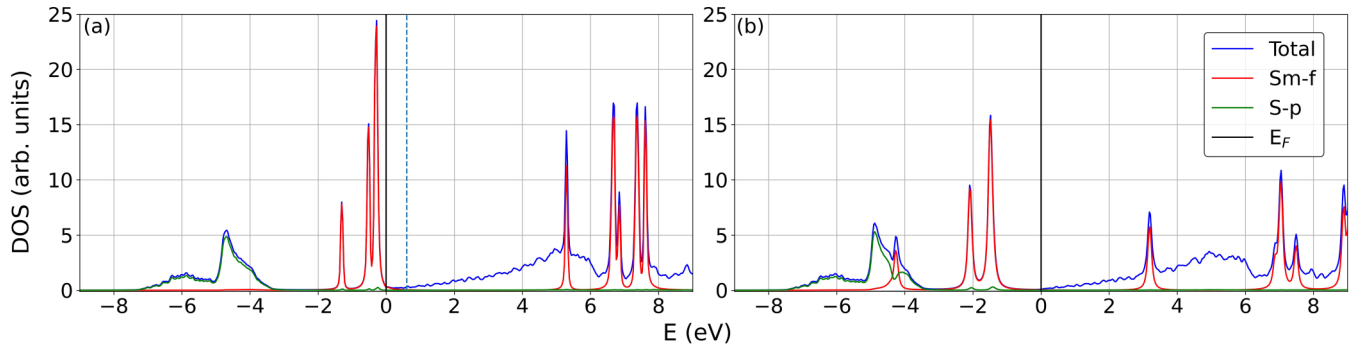


FIG. 5. A comparison between the DOS for different values of Hund’s coupling  $J$  for SmS with  $J = 0.3$  eV and (b)  $J = 0.8355$  eV, adapted from Ref. [33]. The choice of  $J = 0.3$  is based on correctly reproducing the hybridization between Sm-4*f* and S-*p* states and the band gap consistent with experimental observations.

$a$  under ambient pressure with the NEB parameter  $\lambda = 0$  and interpolate both the structural and electronic parameters, i.e., the lattice constant and the double counting, respectively, to what we predict to be the high-pressure metallic ground states corresponding to  $\lambda = 1$ . Along this path, while going from the insulating phase to the metallic phase, there is a regime where the  $f$  states cross the Fermi level [Fig. 6(c)]. This variation of density corresponds entirely to the impurity states confirming that the metallic conductivity in the SmS golden phase originates from the Sm-4*f* states as seen in experiments [52,53]. Additionally along this path, we observe a change in occupancy which follows well the experimentally predicted valence for the insulating and the intermediate valence metallic states [Fig. 6(b)]. This trend in valence remains similar for all three materials. On going to room temperature ( $\beta = 40$ ) and linearly interpolating as before, insulating states of SmX show a maximum change in  $Z$  by 0.031, 0.021, and 0.058, whereas the metallic phases change by 0.004, 0.061, and 0.103, respectively, for SmS, SmSe, and SmTe. This is consistent with the noted small shifts in the DOS at room temperature (Fig. 7), where no qualitative differences in trends were noted. Note that our NEB approach interpolates linearly between the structural and electronic properties of the respective metallic and insulating equilibrium phases corresponding to different lattice constants  $a$  and nominal occupancies  $n_{if}$ , respectively. Our equation of states in these two phases follows the Birch-Murnaghan [47,48] relation, where

the structure is indeed uniquely defined for each chalcogenide, but the transition from metal to insulator can be obtained by many different paths or processes with many combinations of structural deformations and associated electronic transitions. Thus we cannot infer about the possible lowest energy barrier, first-order transitions, or sharp discontinuity in the Sm valence.

However, contrary to expectations, not only does the quasiparticle weight  $Z$  decrease, but also it is nonzero for the observed insulating phases [Fig. 6(a)]. However, when we reach the predicted metallic states for SmSe and SmTe,  $Z$  goes up a little. Although the effective mass is mostly dominated by the mass renormalization due to the  $f$  electrons, it shows that this MIT is not a Mott transition. Based on this behavior, we argue that these are correlated band insulators instead, confirming the ARPES results for SmS [52], where on driving towards the metallic phase the Sm-4*f* state interestingly become even more correlated, and thus we conclude that here  $Z$  is not a measure of transition. In the predicted metallic states, the  $f$  states are weakly hybridized at the Fermi level. Across the MIT, they do cross the Fermi level but do not end up in the metastable configuration. So, the 4*f* states are across the energy barrier that separates these two phases. At some point along the NEB, we are passing through a state which is reminiscent of Kondo lattices. These  $f$  states are, however, very important for transport and the role of SmX as PR materials because if we gate the system, small voltages

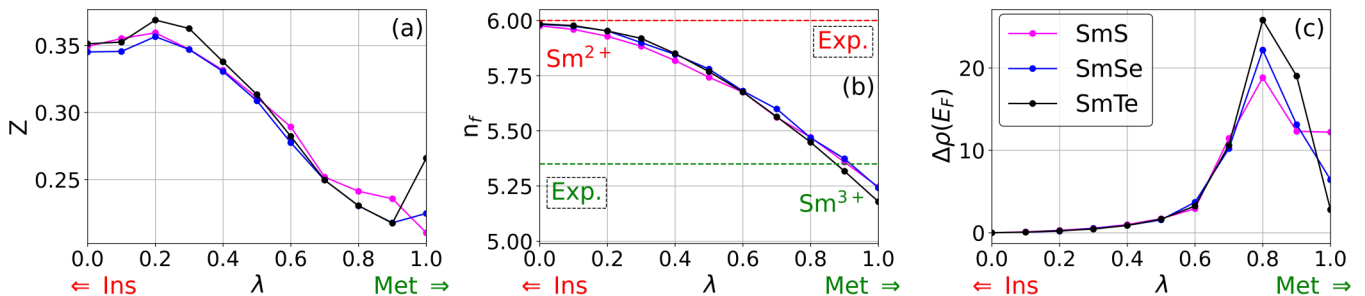


FIG. 6. (a) Total quasiparticle weight  $Z$ , (b) Sm-4*f* electron occupancy  $n_f$ , and (c) total density of states at the Fermi level  $\rho(E_F)$  along the NEB path going from the insulating state (Ins;  $\lambda = 0$ ) to the metallic state (Met;  $\lambda = 1$ ) for SmS, SmSe, and SmTe.

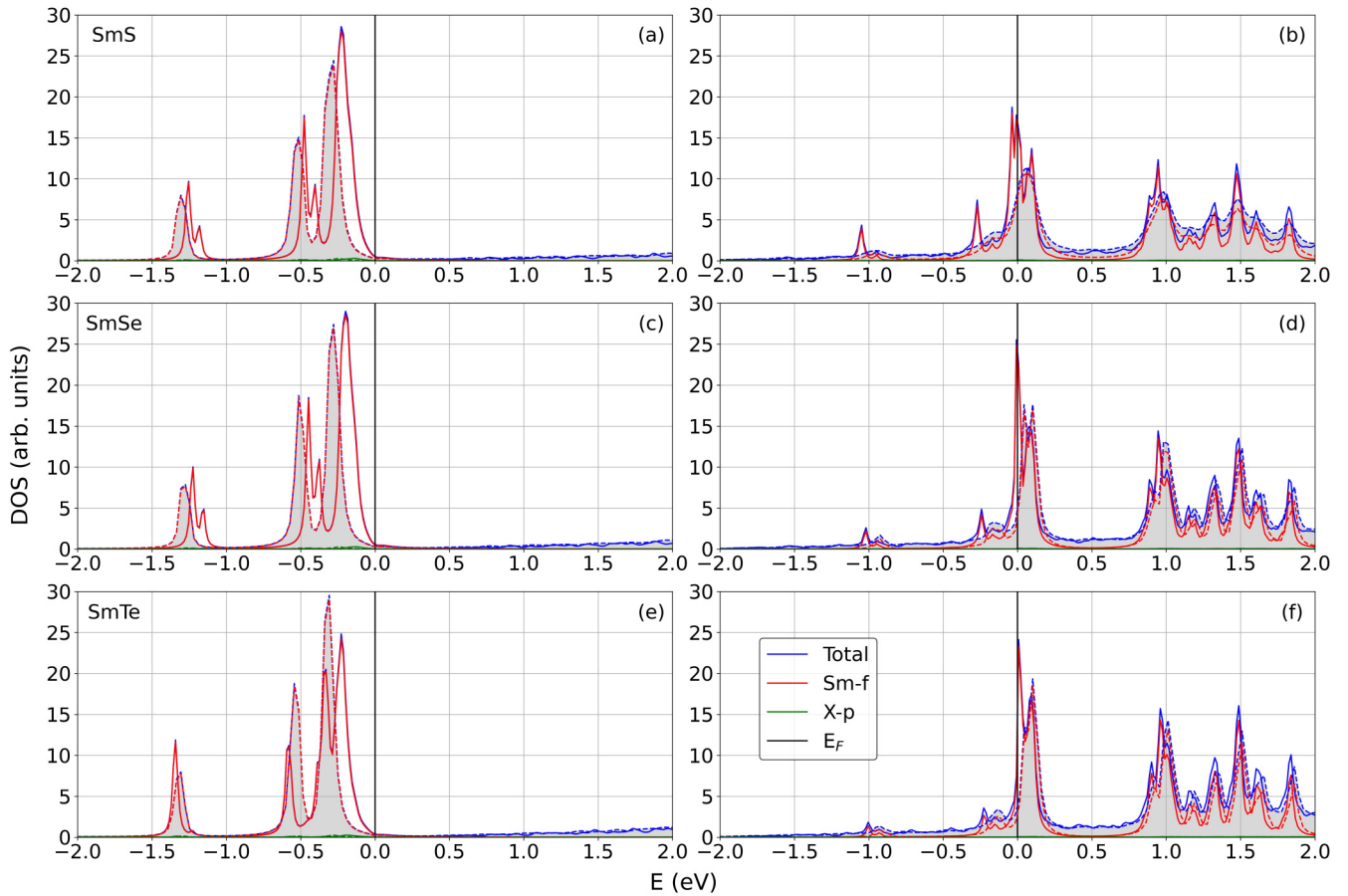


FIG. 7. Left column: difference in the density of states obtained with DFT+DMFT at high temperature ( $T = 0.05$  eV; solid lines, unshaded) and room temperature ( $T = 0.026$  eV; dashed lines, shaded) corresponding to the ambient pressure insulating states for (a) SmS, (c) SmSe, and (e) SmTe. Right column: the high-pressure intermediate valence metallic states for (b) SmS, (d) SmSe, and (f) SmTe. Small shifts in the DOS are observed on lowering the temperature with no qualitative differences in trends compared with the higher temperature.

might suddenly involve the  $f$  states in the conduction and they might start contributing more.

#### IV. CONCLUSION AND DISCUSSION

In conclusion, DFT+DMFT correctly explains the pressure-induced insulator-to-metal transition with a concomitant change in valence in Sm monochalcogenides owing to its access of the fractional electronic occupations. It leads to significant improvements over the predicted values of lattice constants and bulk moduli for the experimentally observed states as a direct result of incorporating the charge and spin fluctuations. We also obtain the multiplet nature of the DOS with excellent experimental agreement in the absence of any long-range interactions or spin-orbit coupling. On doing the NEB, we find that the quasiparticle weight remains finite for the insulating phases, decreases with pressure, and is not an

indication of this transition, thus inferring that this is not a Mott transition. As a result, we classify these materials as correlated band insulators.

#### ACKNOWLEDGMENTS

D.B. acknowledges the support of NPIF Grant No. EP/R512552/1 and the UK EPSRC CDT for CANES Grant No. EP/L015854/1. C.W. and E.P. were supported by Grant No. EP/R02992X/1 from EPSRC. I.R. acknowledges the support of the UK Department for Business, Energy and Industrial Strategy through the UKNQT program. D.B. and I.R. were also supported by the EU Horizon 2020 research and innovation program within PETMEM Project No. 688282. This work was performed using resources provided by the ARCHER UK National Supercomputing Service and the CSD3 facility hosted by the University of Cambridge (Capital Grant No. EP/P020259/1).

- [1] G. E. Moore, *IEEE Solid-State Circuits Society Newsletter* **11**, 33 (2006).
- [2] D. M. Newns, B. G. Elmegreen, X.-H. Liu, and G. J. Martyna, *Adv. Mater. (Weinheim)* **24**, 3672 (2012).
- [3] P. Ciureanu, *Thin Film Resistive Sensors*, Sensors Series (CRC, Boca Raton, FL, 1992).
- [4] H. S. Nalwa, *Ferroelectric and Dielectric Thin Films, Handbook of Thin Film Materials* Vol. 3 (Academic, San Diego, CA, 2002).
- [5] A. Sousanis, D. Poelman, C. Detavernier, and P. F. Smet, *Sensors* **19**, 4390 (2019).
- [6] A. Sousanis, P. F. Smet, and D. Poelman, *Materials* **10**, 953 (2017).
- [7] A. Jayaraman, V. Narayanamurti, E. Bucher, and R. G. Maines, *Phys. Rev. Lett.* **25**, 368 (1970).
- [8] A. Jayaraman, V. Narayanamurti, E. Bucher, and R. G. Maines, *Phys. Rev. Lett.* **25**, 1430 (1970).
- [9] M. B. Maple and D. Wohlleben, *Phys. Rev. Lett.* **27**, 511 (1971).
- [10] P. P. Deen, D. Braithwaite, N. Kernavanois, L. Paolasini, S. Raymond, A. Barla, G. Lapertot, and J. P. Sanchez, *Phys. Rev. B* **71**, 245118 (2005).
- [11] P. Hohenberg and W. Kohn, *Phys. Rev.* **136**, B864 (1964).
- [12] W. Kohn and L. J. Sham, *Phys. Rev.* **140**, A1133 (1965).
- [13] V. N. Antonov, B. N. Harmon, and A. N. Yaresko, *Phys. Rev. B* **66**, 165208 (2002).
- [14] A. Svane, G. Santi1, Z. Szotek, W. M. Temmerman, P. Strange, M. Horne, G. Vaitheeswaran, V. Kanchana, L. Petit, and H. Winter, *Phys. Status Solidi B* **241**, 3185 (2004).
- [15] A. Svane, V. Kanchana, G. Vaitheeswaran, G. Santi, W. M. Temmerman, Z. Szotek, P. Strange, and L. Petit, *Phys. Rev. B* **71**, 045119 (2005).
- [16] L. Petit, Z. Szotek, M. Lüders, and A. Svane, *J. Phys.: Condens. Matter* **28**, 223001 (2016).
- [17] D. C. Gupta and S. Kulshrestha, *J. Phys.: Condens. Matter* **21**, 436011 (2009).
- [18] M. Singh, A. Gour, and S. Singh, *Acta Phys. Pol., A* **123**, 709 (2013).
- [19] S. Kapoor, N. Yaduvanshi, and S. Singh, *Ferroelectrics* **519**, 139 (2017).
- [20] R. Dubey and S. Singh, *J. Mol. Struct.* **1052**, 204 (2013).
- [21] S. Watanabe, *J. Phys. Soc. Jpn.* **90**, 023706 (2021).
- [22] H. L. Skriver, *Phys. Rev. B* **31**, 1909 (1985).
- [23] P. Per Söderlind, P. E. A. Turchi, A. Landa, and V. Lordi, *J. Phys.: Condens. Matter* **26**, 416001 (2014).
- [24] W. Metzner and D. Vollhardt, *Phys. Rev. Lett.* **62**, 324 (1989).
- [25] A. Georges and G. Kotliar, *Phys. Rev. B* **45**, 6479 (1992).
- [26] A. Georges, G. Kotliar, W. Krauth, and M. J. Rozenberg, *Rev. Mod. Phys.* **68**, 13 (1996).
- [27] G. Kotliar, S. Y. Savrasov, K. Haule, V. S. Oudovenko, O. Parcollet, and C. A. Marianetti, *Rev. Mod. Phys.* **78**, 865 (2006).
- [28] J. B. Goodenough, *J. Solid State Chem.* **3**, 490 (1971).
- [29] W. H. Brito, M. C. O. Aguiar, K. Haule, and G. Kotliar, *Phys. Rev. Lett.* **117**, 056402 (2016).
- [30] M. J. Rozenberg, G. Kotliar, H. Kajueter, G. A. Thomas, D. H. Rapkine, J. M. Honig, and P. Metcalf, *Phys. Rev. Lett.* **75**, 105 (1995).
- [31] M. Imada, A. Fujimori, and Y. Tokura, *Rev. Mod. Phys.* **70**, 1039 (1998).
- [32] P. Limelette, A. Georges, D. Jérôme, P. Wzietek, P. Metcalf, and J. M. Honig, *Science* **302**, 89 (2003).
- [33] C.-J. Kang, H. C. Choi, K. Kim, and B. I. Min, *Phys. Rev. Lett.* **114**, 166404 (2015).
- [34] M. C. Payne, M. P. Teter, D. C. Allan, T. Arias, and J. D. Joannopoulos, *Rev. Mod. Phys.* **64**, 1045 (1992).
- [35] S. J. Clark, M. D. Segall, C. J. Pickard, P. J. Hasnip, M. J. Probert, K. Refson, and M. Payne, *Z. Kristallogr.* **220**, 567 (2005).
- [36] J. P. Perdew, A. Ruzsinszky, G. I. Csonka, O. A. Vydrov, G. E. Scuseria, L. A. Constantin, X. Zhou, and K. Burke, *Phys. Rev. Lett.* **100**, 136406 (2008).
- [37] H. J. Monkhorst and J. D. Pack, *Phys. Rev. B* **13**, 5188 (1976).
- [38] E. Plekhanov, P. Hasnip, V. Sacksteder, M. Probert, S. J. Clark, K. Refson, and C. Weber, *Phys. Rev. B* **98**, 075129 (2018).
- [39] J. F. G. Kresse, *Comput. Mater. Sci.* **6**, 15 (1996).
- [40] G. Kresse and J. Furthmüller, *Phys. Rev. B* **54**, 11169 (1996).
- [41] P. E. Blöchl, *Phys. Rev. B* **50**, 17953 (1994).
- [42] G. Kresse and D. Joubert, *Phys. Rev. B* **59**, 1758 (1999).
- [43] J. P. Perdew, K. Burke, and M. Ernzerhof, *Phys. Rev. Lett.* **77**, 3865 (1996).
- [44] S. Steiner, S. Khmelevskyi, M. Marsmann, and G. Kresse, *Phys. Rev. B* **93**, 224425 (2016).
- [45] J. Röhler, in *High Energy Spectroscopy*, Handbook on the Physics and Chemistry of Rare Earths Vol. 10 (Elsevier, Amsterdam, 1987), Chap. 71, pp. 453–545.
- [46] T. Ito, A. Chainani, H. Kumigashira, T. Takahashi, and N. K. Sato, *Phys. Rev. B* **65**, 155202 (2002).
- [47] F. Birch, *Phys. Rev.* **71**, 809 (1947).
- [48] F. D. Murnaghan, *Proc. Natl. Acad. Sci. U. S. A.* **30**, 244 (1944).
- [49] P. Wachter, in *Alloys and Intermetallics, Handbook on the Physics and Chemistry of Rare Earths* Vol. 2 (Elsevier, Amsterdam, 1994), Chap. 19, pp. 507–574.
- [50] T. Le Bihan, S. Darracq, S. P. Heathman, U. G. Benedict, K. Mattenberger, and O. Vogt, *J. Alloys Compd.* **226**, 143 (1995).
- [51] H. Jonsson, G. Mills, and J. C. Karsten, in *Classical and Quantum Dynamics in Condensed Phase Simulations* (World Scientific, Singapore, 1998), pp. 385–404.
- [52] K. Imura, T. Hajiri, M. Matsunami, S. Kimura, M. Kaneko, T. Ito, Y. Nishi, N. K. Sato, and H. S. Suzuki, *J. Korean Phys. Soc.* **62**, 2028 (2013).
- [53] T. Penney and F. Holtzberg, *Phys. Rev. Lett.* **34**, 322 (1975).